

# Computational Analysis of Routine Biopsies Improves Diagnosis and Prediction of Cardiac Allograft Vasculopathy

**Running Title:** Peyster et al.; Digital Pathology Predicts Allograft Vasculopathy

Eliot G. Peyster MD, MSc<sup>1</sup>; Andrew Janowczyk, PhD<sup>2,3</sup>; Abigail Swamidoss, HSDG<sup>2</sup>; Samhith Kethireddy, HSDG<sup>2</sup>; Michael D. Feldman, MD, PhD<sup>4</sup>; Kenneth B. Margulies, MD<sup>1</sup>

<sup>1</sup>Cardiovascular Research Institute, University of Pennsylvania, Philadelphia, PA; <sup>2</sup>Department of Biomedical Engineering, Case Western Reserve University, Cleveland, OH; <sup>3</sup>Department of Oncology, Lausanne University Hospital and Lausanne University, Lausanne, Switzerland;

<sup>4</sup>Department of Pathology & Laboratory Medicine, University of Pennsylvania, Philadelphia, PA

## Address for Correspondence:

Eliot Peyster, MD, MSc  
 Assistant Professor, University of Pennsylvania  
 Advanced Heart Failure and Transplant Medicine  
 Smilow Translational Research building, Rm. 11-113  
 3400 Civic Center Blvd. Philadelphia, PA, 19130  
 Phone: +1 215-554-0993  
 Email: [Eliot.peyster@pennmedicine.upenn.edu](mailto:Eliot.peyster@pennmedicine.upenn.edu)

\*This article is published in its accepted form, it has not been copyedited and has not appeared in an issue of the journal. Preparation for inclusion in an issue of *Circulation* involves copyediting, typesetting, proofreading, and author review, which may lead to differences between this accepted version of the manuscript and the final, published version.

## Abstract

**Background:** Cardiac allograft vasculopathy (CAV) is a leading cause of morbidity and mortality for heart transplant recipients. While clinical risk factors for CAV have been established, no personalized prognostic test exists to confidently identify patients at high vs. low risk of developing aggressive CAV. The aim of this investigation was to leverage computational methods for analyzing digital pathology images from routine endomyocardial biopsies (EMB) to develop a precision medicine tool for predicting CAV years before overt clinical presentation.

**Methods:** Clinical data from 1-year post-transplant was collected on 302 transplant recipients from the University of Pennsylvania, including 53 ‘early CAV’ patients and 249 ‘no-CAV’ controls. This data was used to generate a ‘clinical model’ (ClinCAV-Pr) for predicting future CAV development. From this cohort, n=183 archived EMBs were collected for CD31 and modified trichrome staining and then digitally scanned. These included 1-year post-transplant EMBs from 50 ‘early CAV’ patients and 82 no-CAV patients, as well as 51 EMBs from ‘disease control’ patients obtained at the time of definitive coronary angiography confirming CAV. Using biologically-inspired, hand-crafted features extracted from digitized EMBs, quantitative histologic models for differentiating no-CAV from disease controls (HistoCAV-Dx), and for predicting future CAV from 1-year post-transplant EMBs were developed (HistoCAV-Pr). The performance of histologic and clinical models for predicting future CAV (i.e. HistoCAV-Pr and ClinCAV-Pr, respectively) were compared in a held-out validation set, before being combined to assess the added predictive value of an integrated predictive model (iCAV-Pr).

**Results:** ClinCAV-Pr achieved modest performance on the independent test set, with area under the receiver operating curve (AUROC) of 0.70. The HistoCAV-Dx model for diagnosing CAV achieved excellent discrimination, with an AUROC of 0.91, while HistoCAV-Pr model for predicting CAV achieved good performance with an AUROC of 0.80. The integrated iCAV-Pr model achieved excellent predictive performance, with an AUROC of 0.93 on the held-out test set.

**Conclusions:** Prediction of future CAV development is greatly improved by incorporation of computationally extracted histologic features. These results suggest morphologic details contained within regularly obtained biopsy tissue have the potential to enhance precision and personalization of treatment plans for post-heart transplant patients.

**Key Words:** Image Analysis; Digital Pathology; Allograft Vasculopathy; Heart Transplant; Machine Learning; Risk Prediction

**Non-Standard Abbreviations and Acronyms:** CAV, cardiac allograft vasculopathy; EMB, Endomyocardial Biopsy; DSA, Donor specific Antibody; ISHLT, International Society of Heart and Lung Transplantation; PrE-CAV, Pre-Early-onset Cardiac Allograft Vasculopathy; No-CAV, No early onset Cardiac Allograft Vasculopathy; DC, Disease Control; BMI, Body Mass Index; LDL, Low Density Lipoprotein; CMV, Cytomegalovirus; PRA, Panel Reactive Antibody; OHT, Orthotopic Heart Transplant; LVEF, Left Ventricular Ejection Fraction; HLA, Human Leukocyte Antigen; BUN, Blood Urea Nitrogen; AMR, Antibody Mediated Rejection; DAB, 3,3' Diaminobenzidine; LOOCV, Leave-One-Out Cross Validation; AUROC, Area Under Receiver Operating characteristic Curve; HistoCAV-Dx, Histologic Cardiac Allograft Vasculopathy Diagnostic model; ClinCAV-Pr, Clinical risk factor future Cardiac Allograft Vasculopathy Prediction model; HistoCAV-Pr, Histologic future Cardiac Allograft Vasculopathy Prediction model; iCAV-Pr, Integrated histologic/clinical risk factor future Cardiac Allograft Vasculopathy Prediction model



## Clinical Perspective

### What is new?

- For the first time, quantitative morphologic biomarkers extracted from routine heart transplant recipient biopsy samples were used to predict cardiac allograft vasculopathy years before overt disease onset in a retrospective cohort.
- Morphologic biomarkers describing the proliferation of interstitial fibers and the ‘cellularity’ of the intra- and peri-vascular space demonstrated the strongest predictive potential for future vasculopathy development.
- A novel and intuitive integrated modeling approach combining computationally-extracted, tissue-level, morphologic biomarkers with conventional, patient-level risk factors demonstrated clear synergy, with performance for predicting allograft vasculopathy that far exceeds models relying on either individual data source.



### What are the clinical implications?

- Validated performance in an independent test set suggests that a deeper investigation of regularly obtained and readily-accessible pathology specimens and clinical data can be used for allograft vasculopathy prediction as early as 1-year post-transplant.
- Highly sensitive and specific predictions of allograft vasculopathy as demonstrated in this research could enable clinicians to tailor both screening and preventative therapeutic strategies to individual risk profiles, minimizing cost and harm from unnecessary testing while maximizing the benefit of more intensive regimens.

## Introduction

Heart transplantation remains the first line treatment for eligible patients with end-stage heart disease. Each year, more than 4000 heart transplants are performed worldwide<sup>1</sup>, offering markedly improved quality of life and longevity for the vast majority of recipients. However, transplanted hearts do not last forever, with recipient immune responses against the allograft posing a continuous threat that requires vigilant surveillance and careful medical management. While acute episodes of allograft rejection are the most apparent mechanism of allo-immune injury experienced by transplant recipients, indolent, immune-mediated vascular injury, known as cardiac allograft vasculopathy (CAV), represents the leading cause of allograft failure after the first-year post-transplant<sup>2-4</sup>.



Despite being a leading cause of morbidity and mortality for transplant recipients, CAV surveillance strategies remain highly variable across centers, with little progress being made in tailoring surveillance strategies to individual patient risk profiles<sup>4-6</sup>. While the usage of regular endomyocardial biopsy (EMB) remains the universal standard for acute rejection monitoring, for CAV monitoring, some centers opt for less invasive approaches with annual stress testing, with others opting for a more invasive approach with annual or periodic coronary angiography. Regardless of the specific surveillance approach employed, all current methods for CAV detection rely on repurposing techniques initially developed for traditional coronary artery disease. As such, these techniques focus primarily on estimating the flow of blood through large, epicardial coronary arteries. Despite the macroscopic focus of commonly used CAV diagnostics, the pathobiology of CAV involves not only narrowing of the large muscular arteries of the heart, but also significant (and often antecedent) microvascular inflammation and injury to the capillaries and smaller pre-capillary arterioles<sup>3,4,7,8</sup>. The importance of microvascular injury to end-organ function has

been demonstrated in pathology studies of the native heart<sup>9-11</sup>, the transplanted heart<sup>8,12-14</sup>, and in other solid organ transplants<sup>15-17</sup>. Moreover, pathologic studies have consistently demonstrated that histologically apparent changes to the microarchitecture of vessels and tissue precede and predict eventual macroscopic findings and overt graft dysfunction<sup>13,17,18</sup>. Yet despite several decades of published literature describing histopathologic changes consistent with microvascular disease in CAV, no standardized, objective framework for measuring these changes has been developed.

Multiple studies have attempted to identify clinical metrics that might be predictive of future CAV<sup>5,19-24</sup>. The most successful of these efforts have attempted to incorporate not only baseline donor and recipient characteristics, but also several post-transplant metrics describing a predisposition to allo-immunity (including a history of acute cellular rejection or donor specific antibodies (DSA) in the first year). However, the performance on an individual patient level of these clinical metrics remains uncertain<sup>25</sup>, and consequently, the clinical impact of these efforts has been limited. To date, no study has attempted to pursue a rigorous analysis of the histologic data contained within routine EMB tissues as a means of generating better, more personalized CAV risk assessments. This has been considered can be considered unmet need<sup>26</sup> and an emerging opportunity<sup>27</sup>, given the promise computational digital pathology analysis has shown for providing clinically valuable predictions in heart transplant medicine<sup>28-30</sup> and beyond<sup>31-35</sup>.

In this proof-of-concept study, we perform computational image analysis of digitized EMB histology slides using an interpretable, ‘hand-crafted’ methodology in order to discover and measure novel histologic biomarkers associated with the development of CAV. Further, we utilize these biomarkers, along with relevant clinical data, to develop an integrated clinical and histologic model for predicting the development of early, severe CAV.

## Methods

The source code for the image analysis pipeline is freely available on Github (<https://github.com/choosehappy/iCAV-Pr>). Additional data are available from the corresponding author at reasonable request.

### **Study Cohort and Design:**

The study cohort consisted of patient records and archived clinical histology samples from the University of Pennsylvania. Figure 1 provides a flow diagram outlining the experiment design. Briefly, cohort generation started with a review of transplant recipient clinical data extracted from the electronic health records from 2007-2020 (n=706 patients). Detailed clinical records at one-year post-transplant, as well as CAV outcomes data, were collected for each patient. Based on chart review, n=53 Pre-‘Early-CAV’ (PrE-CAV) patients were identified, defined as patients with an angiographic diagnosis of CAV with an International Society of Heart and Lung Transplantation (ISHLT) grade of 2 or 3 (denoting angiographic evidence of focal severe stenosis or diffuse disease with evidence of allograft dysfunction)<sup>19</sup> occurring within five years of transplantation. An additional n=249 ‘No-CAV’ patients were identified, defined as having no history of positive stress-testing or angiographic evidence of CAV at six-years post-transplant. Every patient with adequate clinical records who met the appropriate study definitions for ‘PrE-CAV’ or ‘No-CAV’ was included in the final cohort. Table 1 provides the clinical characteristics of the full study cohort (n=302).

For the development of an automated histology analysis pipeline, we identified surveillance EMB biopsy samples free of rejection that were obtained closest to the one-year post-transplant anniversary. We retrieved n=50 EMB tissue blocks from PrE-CAV patients, and n=82

EMB tissue blocks from No-CAV patients from the Pathology archives at the University of Pennsylvania. In addition, n=51 EMB tissue blocks from biopsy procedures performed at the time of definitive coronary angiography diagnosing patients with grade 2 or 3 CAV were also obtained to represent ‘disease control’ (DC) histology samples (these patients were not necessarily PrE-CAV patients, but instead are defined by the availability of EMB tissue at the time of definitive CAV diagnosis). Table 2 provides relevant biopsy sample characteristics for the cases undergoing automated histologic analysis. Access to clinical data and archival tissue were approved by the University of Pennsylvania institutional review board, with waiver-of-consent authorized by 45 CFR 46.116(d) and 45 CFR 164.512(i).

### **Histology Slide Preparation**



All samples were fixed in 4% paraformaldehyde and embedded in paraffin at the time of EMB procedure, as per routine care. Residual EMB tissue blocks were retrieved from pathology archives, with two serial 10 $\mu$ m sections cut from each block. One section was stained with Movat’s pentachrome (a modified trichrome stain permitting discrimination of ground-substance/proteoglycans from collagen and reticular fibers), while the other underwent immunohistochemistry with CD31 (Ab28364, Abcam, Cambridge, UK, with 3,3'-Diaminobenzidine[DAB] labeling) and hematoxylin to highlight endothelial cells. Digital histology images were generated via whole-slide scanning at 40x magnification using either an Aperio ScanScope or a Hamatsu S360 slide scanner. Two different scanners were utilized to enable assessment of image analysis pipeline performance on different devices – an important source of bias in digital pathology<sup>36</sup>. Figure 2 shows digital histology images for No-CAV, PrE-CAV, and DC EMBs for each stain.

## **Image Quality Control**

Image quality control is an essential component of digital image analysis research. Digitized slides underwent quality control assessments using HistoQC, an open-source, automated digital pathology tool for identifying artifacts and measuring slide quality which we have successfully applied to previous investigations in cardiac histology<sup>29, 37</sup>.

## **Overview of Image Analysis Workflow**

The image analysis workflow focused on extracting relevant morphologic features from the CD31 and Movats stained images separately, prior to combining the feature-sets to generate quantitative variables during data analysis. Our feature selection approach was informed by decades of published observations on interstitial expansion/remodeling in the setting of subacute/chronic allograft inflammation<sup>38-41</sup>, on endotheliitis/endothelial cell thickening in CAV<sup>8,42,43</sup>, and on cellular proliferation and migration in the vessel wall or perivascular space during indolent allo-immunity<sup>3,42,44</sup>. Using this often observational information as inspiration, we then attempted to extract measurable features that capture these phenomena. Analysis was conducted on whole-slide images, with specific workflows summarized below and in Figure 3. A detailed, step-by-step overview of image analysis methods is provided in the Supplemental Methods.

### **CD31 Workflow**

The primary purpose of CD31 slides was to facilitate accurate extraction of morphologic biomarkers describing the microvasculature. The open-source digital pathology tool QuPath (V.0.2.3) was employed for raw image data extraction from CD31 slides, with a focus on identifying DAB-stained endothelial cells and hematoxylin-stained nuclei. Stain deconvolution algorithms enabled reliable separation of areas containing specific – and even overlapping – stain-

colors<sup>45</sup>. Following stain deconvolution, three pixel-level classifiers were created for assigning pixels to (a) the CD31/DAB class, (b) the hematoxylin class, (c) remaining tissue class. Python (using the Shapely and Pandas libraries) was used for quantitative feature development via the measurement of areas, counts, densities, and specific arrangements of classified pixels. To ensure a comprehensive and nuanced evaluation of the cardiac microvasculature, and due to uncertainty over which type/size of microvessel might provide the most valuable predictive information, several ‘binning’ strategies for sub-classifying vascular (e.g. DAB-staining) objects by size were explored. This involved first removing the extreme outliers of size (DAB+ objects with areas in the top 0.1% of the entire cohort), which represent either small off-target staining objects or rare, sporadically distributed large vascular objects at the border between micro- and macro-vessels (eg. diameters $\geq$ ~50-100 $\mu\text{m}$ )<sup>11</sup>. Next, DAB regions were binned using three different approaches: (a) statistical criteria (i.e., 0.5, 1, 1.5, 2, 3, and  $>3$  standard deviations away from mean), (b) evenly-spaced quartiles, and (c) previously-defined anatomical criteria<sup>8</sup>, as summarized in Supplemental Figure S.1 and Table S.1. Next, in order to assess the perivascular environment, detection of nuclei within a small area around DAB+ regions was performed, which involved slightly dilating DAB regions (proportional to their size) and counting cells falling within this expansion. A full set of quantitative measurements were generated for the total DAB+ object population across the whole slide and for each size bin from each binning approach.

## Movats Workflow

The primary purpose of Movats staining was to achieve reliable quantitation of myocytes and various stromal fiber types within EMB tissue samples. Movat’s Pentachrome stained slides include differentially stained regions of myocytes, collagen, proteoglycans, and elastin. Thresholds in the HSV color space were employed to create individual binary masks for each stain color/fiber

type. After modest post-processing (e.g., hole filling and dilation), Python's NumPY library was used to calculate the total area for each of the binary masks per slide. Recognizing that dense areas of stroma on the endocardial surface or at areas of prior biopsy site may have different implications from interstitial stromal proliferation, we also performed sub-analysis of stromal fiber content within the myocardial compartment alone (e.g., the areas of tissue which contain significant myocyte density). This was achieved via disc-dilation of the myocyte segmentation results, which created a confluent mask encompassing the myocyte-containing regions of tissue. Using this 'myocardium mask', the different stromal fibers could be measured to assess their relative contributions to interstitial changes in the tissue.

## Data Analysis and Statistical Methods



### *Image Feature Selection and Morphologic Model Construction*

The measurements extracted via the image analysis workflow describe the sizes, areas, and counts of various morphologic features. After extraction, the CD31 and Movats features are merged to derive variables for predictive modeling by calculating different cell/tissue-type/object ratios and via different normalization methods (e.g., dividing by total tissue area or myocardium area). In total, 680 quantitative variables characterizing the morphology of EMBs were computed for each case. These variables describe interstitial composition and proliferation, myocyte density, total vascular density, the proportions of vessels of different sizes, and the cellular abundance both within vessels and in the immediate perivascular space (Figure 4). These features were subsequently used to produce two distinct classification models – a 'Diagnostic Model' (HistoCAV-Dx) to differentiate No-CAV EMBs from DC EMBs (total cohort n=133), and a 'Morphologic Predictive Model' (HistoCAV-Pr) to differentiate No-CAV EMBs from PrE-CAV EMBs (total cohort n=132). For each modeling task, the cohorts were divided into training sets

containing ~66% of the cases for variable selection and model calibration, and a held-out testing set containing ~34% of the cases for model validation.

Using only the training set for model development, variables were initially ranked by univariate T-test and Kruskall-Wallis values for each classification task (diagnosis and prediction). Features with p-values <0.05 were then included in multivariable logistic regression models, with model optimization occurring via backwards elimination. Recognizing that univariate ranking of features can exclude variables with potentially important predictive value when considered in the context of multivariable models<sup>46</sup>, variables initially excluded due to higher p-values were reevaluated via forward stepwise selection based on achieving a multivariable p value <0.165 (a slightly lenient approximation of the Akaike Information Criteria)<sup>46,47</sup>. For model optimization, leave-one-out cross-validation (LOOCV) was employed, assessing accuracy, area under the receiver operator characteristic curve (AUROC), and degree of overfit within the training set<sup>48</sup>. Selection of the optimal classification cutoff points for accuracy testing within the training sets were guided by the Liu method<sup>49</sup>. After locking-down final model parameters for study histologic models, the models were next applied to the held-out test sets, with model performance assessed via AUROC, accuracy, sensitivity, and specificity. All statistical analyses were performed in Stata v.15.0 (StataCorp, LLC).

#### *Clinical Risk Factor Modeling*

Comprehensive clinical phenotyping of all n=302 patients was performed to enable creation of a ‘Clinical Prediction Model’ (ClinCAV-Pr) for differentiating PrE-CAV patients from No-CAV patients based on baseline and 1-year post transplant data. Clinical data included detailed donor and recipient medical history, data pertaining to the transplant event, pre- and post-transplant clinical immunology data, and post-transplant outcomes data (including standard histologic



assessments of surveillance allograft biopsies). In total, 85 clinical variables were available for predictive modeling. As described with the morphologic data above, the clinical data cohort was divided into a training set containing approximately two-thirds of the cases (n=207), and a held-out testing set containing one-third (n=95). To prevent data leakage in the combined model, cases contributing EMB tissue for morphologic analysis were assigned to the same group (training vs testing) as they were for generating and validating the HistoCAV-Pr Model. Variable selection for ClinCAV-Pr was informed by a recent publication which validated six multivariable risk factors for CAV (donor age, donor sex, donor cigarette use, recipient LDL cholesterol at 1-year post-transplant, presence of +DSA at 1-year, and history of cellular rejection at 1-year)<sup>5</sup>, utilizing bidirectional step-wise selection from this six-variable starting point, with variables kept in the model if they achieved a multivariable p-value <0.165. As described above, LOOCV was performed to assess ClinCAV-Pr performance in the training set and to optimize classification cutoff points prior to deploying in the held-out test set. Final ClinCAV-Pr performance in the test set was assessed as described above.

#### *Integrated Prediction of Early CAV*

The incremental benefit of combining clinical risk factors and morphologic biomarkers was assessed in two ways: 1) via simple, two variable logistic regression using the classification probability outputs from ClinCAV-Pr and HistoCAV-Pr models, and 2) by performing backwards elimination and logistic regression using the combined 17 variables from the two modeling approaches. The performance of the two integrated modeling approaches for differentiating No-CAV patients from PrE-CAV patients in the training set were compared, with the model with higher averaged AUROC and accuracy on LOOCV being selected as the final ‘histo-clinical’ Integrated CAV prediction model (iCAV-Pr) for validation testing in the held-out test set. As

already mentioned, the test sets for ClinCAV-Pr and HistoCAV-Pr were congruent, enabling generation of a final iCAV-Pr model that can undergo fair statistical performance comparisons with the baseline models.

### **Pre-specified Secondary Analyses**

Several secondary analyses were performed to further characterize and contextualize performance of study models. As described in the ‘Clinical Risk Factor Modeling’ section above, six clinical risk factors which had demonstrated multivariable significance in a recent large, multicenter CAV study served as the starting point for ClinCav-Pr development. In order to permit comparison of previously identified risk factors to this study’s optimized ClinCAV-Pr, we trained and tested the performance of an additional clinical model incorporating just these six previously-validated risk factors within our study cohort (Supplemental Figure S.3). For the HistoCAV-Pr model, a supplemental analysis comparing classification error rates by the historical ISHLT cellular rejection grade was performed (Supplemental Table S.6). Additionally, a comparison of HistoCAV-Dx and HistoCAV-Pr model performance between slides scanned on the two different slide scanner machines was performed to assess resilience of the feature extraction pipeline to variations in lab equipment (Supplemental Table S.7). Findings from all supplemental analyses are presented in full in the Supplemental Results.

## **Results**

### **Morphologic Diagnostic Model for CAV: No-CAV vs. Disease Controls**

After feature selection as described above, the final HistoCAV-Dx model for discriminating DC tissue samples (obtained at the time of definitive CAV diagnosis) from No-CAV EMB samples

(obtained at 1-year post-transplant) incorporated 11 variables. These included three morphologic biomarkers describing stromal – and in particular, collagen – proliferation both within and outside the myocardial compartment, one describing decreased overall vascular density of the tissue, five describing the distribution of total nuclei within vs. outside the microvessels, and two describing increased cellular density in the perivascular space of larger capillaries and small pre-capillary arterioles (~25-95 $\mu\text{m}^2$ ). Figure 4 provides visual examples of different classes of morphologic biomarkers, while specific model variables with multivariable p values, odds ratios, and annotated descriptions are presented in Supplemental Table S.8. As shown in Figure 5, the HistoCAV-Dx Model for CAV achieved excellent performance after LOOCV in the training set, with an AUROC of 0.91 and an overall accuracy of nearly 88%. On the held-out test set, there was minimal decrement in performance, with an identical AUROC of 0.91 and an accuracy of 86.7%. This suggests sufficient model training, leading to good generalizability without evidence of notable over-fitting.

### Clinical Risk Factor Modeling

ClinCAV-Pr, for predicting PrE-CAV, included seven clinical risk factors: actively treated recipient diabetes at 1-year ( $p=0.071$ ), recipient body mass index at one-year post transplant ( $p=0.087$ ), recipient low-density lipoprotein at one year ( $p=0.005$ ), a history of high-grade cellular rejection or treated rejection in first year ( $p=0.16$ ), the percentage of biopsies in the first year with Quilty lesion ( $p=0.059$ ), donor proteinuria ( $p=0.018$ ), and donor coronary angiography score ( $p=0.006$ ). It should be noted that donor coronary angiography score, which is a variable derived from the validated EuroTransplant Heart Donor Score50, incorporates and is partially co-linear with donor age, which has consistently been found to be a risk factor for CAV in prior research<sup>5,24,51</sup>. Model performance after cross validation is summarized in Figure 6. Overall,

the clinical model for predicting future development of PrE-CAV achieves modest performance on LOOCV in the training set (AUROC 0.745, accuracy 70.5%), with similar (albeit slightly worse) in the held-out test set (AUROC 0.705, accuracy 66.3%). Positive predictive value is evidently poor at 34% in the training set and 28% in the test set. The apparently strong true-negative rate derives largely from an imbalanced cohort, and overall sensitivity and specificity are both limited at 63% and 67% respectively in the test set.

### **Morphologic Predictive Model for CAV: No-CAV vs. PrE-CAV biopsies**

The HistoCAV-Pr Model for discriminating between 1-year post-transplant EMB samples from PrE-CAV patients vs. No-CAV patients incorporated 10 variables. These included morphologic biomarkers describing (non-collagen) stromal proliferation, total microvessel-staining-area-to-myocyte-staining-area ratio, the proportion of the total microvasculature count and area accounted for by microvessels of different size-bins (with results suggesting a decrease in smaller microvessel count and an increase in larger microvessel relative staining area), and a variable characterizing the cellular density in the perivascular spaces surrounding pre-capillary arterioles (vessels  $\sim 65\mu\text{m}^2$ ). Visual examples of different morphologic biomarker classes are presented in Figure 4, and specific HistoCAV-Pr variables with multivariable p values, odds ratios, and annotated descriptions are presented in Supplemental Table S.9, and representative examples of No-CAV and PrE-CAV slides can be examined for qualitative differences in microarchitecture by referring back to Figure 2. As shown in Figure 6, the HistoCAV-Pr Model for PrE-CAV prediction achieved good performance on LOOCV in the training set, with an AUROC of 0.864 and an accuracy of 80.8%. In the held-out test set, model performance was similar, with an AUROC of 0.80 and an accuracy of 81.6%. Overall, this performance represents an improvement compared to ClinCAV-

Pr in overall performance, with a marked improvement in positive predictive value (75% vs. 27%, p=0.016).

### Integrated CAV Prediction

The final, integrated iCAV-Pr model for PrE-CAV prediction deployed for validation testing was a simple, 2-variable logistic model incorporating the prediction probabilities of ClinCAV-Pr and HistoCAV-Pr models. This model achieved excellent predictive performance after LOOCV in the training set, with an AUROC of 0.939 with an accuracy of 87.5%. Performance of the final iCAV-Pr model was essentially identical in the held-out test set as compared to the training set, with an AUROC of 0.933 and an accuracy of 88.6%, suggesting reasonable model saturation during training and good generalizability. As shown in Figure 6, the iCAV-Pr model demonstrated incremental improvement in AUROC and predictive accuracy within a congruent set of test cases over either constituent model. Statistical comparison of accuracy and AUROC results unambiguously confirms that the addition of morphologic biomarkers adds significant improvements in CAV prediction over traditional clinical risk factors (p=0.005 for accuracy, p=0.009 for AUROC). Interestingly, the final iCAV-Pr model using just the predictive probabilities of ClinCAV-Pr and HistoCAV-Pr as model inputs outperformed a model developed via backwards-elimination using all 17 variables from the final ClinCav-Pr and HistoCAV-Pr models (this 12-variable model achieved an AUROC of 0.87 and an accuracy of 85% after LOOCV, see Supplemental Supplemental Table S.10).

## Discussion

In this manuscript, we have presented compelling findings supporting the utility of EMB tissue analysis for diagnosing and predicting CAV. The quantitative digital pathology method deployed in his work enabled not only the characterization of morphologic biomarkers associated with advanced CAV, but also the discovery of novel biomarkers which are present in EMB samples years before overt CAV development. These predictive morphologic biomarkers were not only out-performed traditional clinical risk factors, but were also orthogonal to them, enabling superior CAV risk assessments when morphologic predictors and clinical predictors were combined.

The present work joins a small but growing body of research deploying computer-assisted histology workflows within cardiovascular medicine<sup>27-30, 52, 53</sup>. Recent efforts have focused on diagnostic pipelines, evaluating cardiac tissue in order to better describe disease states as they currently exist. Specifically within cardiac transplant, several studies have used quantitative analyses to examine transplant EMBs in recent years. However, these works largely focused on acute rejection grading, either trying to develop automated systems to complete this task more reliably<sup>29,53</sup>, or piloting more expensive and complex in-situ analyses to aid in discerning more benign vs. more serious immune processes<sup>30</sup>. This work differs from these prior efforts, focusing on using clinical EMBs to predict a distant future outcome.

Prior research in cardiac digital pathology has involved both ‘deep learning’ methods which prioritize model performance over model interpretability<sup>28,54</sup>, as well as ‘hand-crafted’ methods which utilize supervised feature extraction in order to provide both performance and explanation<sup>29</sup>. The current manuscript relies on a hand-crafted approach, and while this may come at a small decrement in model performance as compared to deep learning methods, the reliance on explicitly defined and demonstrable morphologic features both improves model acceptance and

also enables a glimpse into underlying biology that cannot be elucidated using more opaque deep learning methods. For example, the importance in both morphologic models of image features describing the cellularity of the perivascular space around pre-capillary arterioles highlights an area for deeper mechanistic study. While endotheliitis and endothelial hyperplasia/proliferation are recognized as histologic features of CAV, our results suggest that these may be both early (occurring as soon as 1-year post transplant) and persistent finding (present at the time of CAV diagnosis) findings. Investigations exploring the identity, function, and movement of these cells may lead to a more comprehensive understanding of CAV pathogenesis, and to new strategies for preventing or interrupting its development. Additionally, further study into the perivascular cellular environment may have implications for other diseases affected by cardiac microvascular dysfunction, such as diabetes or heart failure with preserved ejection fraction.



From a clinical perspective, though CAV is a disease with existing treatment and prevention strategies, the application of these strategies lack both timeliness and precision. Thus, a key unmet need in CAV mitigation is personalized risk-stratification capable of confidently describing where a patient will be rather than where they are right now. A recent prospective observational study attempted to address this need using a large, international cohort for modeling patient CAV trajectories<sup>5</sup>. While the scale and rigor of that work is commendable, reliance on a relatively small set of traditional clinical variables (six total donor/recipient risk factors) has raised legitimate concerns over whether such an approach can truly provide confident predictions at the individual patient level<sup>25</sup>. These concerns arise not from the excellent false negative rate of their CAV trajectory model, but rather from the relatively low confidence with which the model predicts clinically serious CAV trajectories<sup>25</sup>. In the present experiment, both the final ClinCAV-Pr model and the clinical dataset from which it is derived have substantial overlap with the risk factors used

in this prior CAV trajectory study. Indeed, our results confirm their fundamental findings – that statistical modeling of donor/recipient cardiovascular risk factors, along with early post-transplant evidence of allo-immune activity, has predictive value. However, our results also validate the aforementioned concerns regarding high false-positive rates when relying on clinical variables alone. If models like the ClinCAV-Pr (or the 6-variable model we developed using the prior publication’s validated risk factors which had even poorer statistical performance) were deployed clinically, this could translate to a substantial iatrogenic harm through escalations in immunosuppression and invasive surveillance for patients who are unlikely to benefit. Thus, the clear strength of the present research is in recognizing the value of broad clinical risk factors, while also acknowledging the need to look beyond traditional risk factors via advanced morphologic analysis of routinely acquired EMB tissues. The end-result of this integrated approach is a predictive assay that looks deeply at tissue, but which also contextualizes the fine-detail of tissue-level findings with pre-test probabilities determined through patient-level risk factors. While conceptually intuitive, the integrative approach employed in this manuscript represents a novel and promising paradigm within cardiovascular (and transplant) medicine.

Despite the strong performance of study histologic models, misclassifications still occurred in each experiment. Anticipating that some degree of misclassification was inevitable, we pre-specified several analyses designed to explore potential contributing factors. Specifically, we conducted analyses to test whether the ISHLT grade, the presence of Quilty, or the presence of prior biopsy site artifacts might affect model performance. These analyses (provided in the supplement) show no significant differences in traditional histology parameters between misclassified and correctly classified EMBs, providing no clear explanation for misclassifications and instead suggesting that the histologic models function in a largely ‘grade-agnostic’ fashion.

Interestingly, ClinCAV-Pr performed essentially as expected on cases incorrectly classified by the HistoCAV-Pr Model, achieving an accuracy of 65% and suggesting that clinical risk factors were not substantially different in the misclassified group. It is possible that tissue or stain quality impacted classification performance, with slides that were outliers in certain quality metrics contributing to classification errors. If this were the case, it would represent a problem that could potentially be solved by increasing the size of the training set to enable models to learn on a broader spectrum of tissue/stain quality. Beyond issues of slide quality, it is also possible that some misclassifications are the result of factors beyond model bias or model training-set size/content. Sampling error is a recognized issue in all histologic fields, and certainly could contribute to misclassification through random sampling of a region of tissue that does not reflect the majority of the myocardium. Additionally, it is worth considering that the allo-immunity leading to CAV is not a static process, and that progression from healthy myocardium to diseased myocardium is neither a continuous process nor a process with a standardized starting time. Patients with evidence of early tissue damage and ongoing allo-immunity at 1-year may sometimes stabilize with adjustments in immunosuppression, improvements in compliance, or the development of ‘accommodation’ in the allograft<sup>55</sup>. On the other hand, patients who do not manifest significant allo-immunity in the first year may experience reductions in immunosuppression or sensitizing events that predispose them to later allo-immune activation and consequent development of CAV. For these reasons, ‘perfect’ CAV prediction based on one-year post-transplant data may not be possible.

As with all experiments, the findings reported in this manuscript should be interpreted in the context of the study’s limitations. The most prominent among these is the size and scope of the study cohort. As a modestly sized, single-center investigation, the findings remain exploratory

and the generalizability of study models remains unsettled. While strong validation results on held-out test sets, along with consistent performance across two different scanning devices and two different slide-processing batches provides some confidence in the generalizability of the pipeline, further external (and, ideally, prospective) validation represents an important next step on the path to clinical translation. Such external validation efforts should focus not only on including data from multiple centers, but would ideally also incorporate additional forms of CAV diagnostic testing such as Intravascular ultrasound. While angiography with intravascular ultrasound is invasive and technically challenging, it can both aid in contextualizing our morphologic biomarkers and in identifying the best populations (and timing) for incorporating digital pathology versus invasive angiographic CAV screening approaches. It should also be noted that while this study utilized EMB tissues as already collected during routine clinical care, the staining for CD31 and Movats pentachrome are not always routine staining for clinical EMB samples. Whether a quantitative histology pipeline for CAV which utilizes only routine H&E stained slides would perform as well remains unsettled. If additional stains are indeed required for best predictive results, then the added time and expense of slide processing would have to be considered an additional challenge for clinical translation. However, this one-time staining cost is not substantial, is far cheaper than invasive testing like intravascular ultrasound, and could potentially be offset by the reduced frequency of stress testing/angiography for patients identified as low-risk.



## Conclusions

We demonstrate that advanced digital pathology methods can identify early microvascular manifestations of CAV with high sensitivity and specificity. Moreover, a model which combines digital pathology ‘morphologic biomarkers’ with conventional clinical risk factors enables the

identification of patients who will develop aggressive CAV years before overt disease onset. If replicated in an external cohort, our integrated approach to CAV prediction could open a new frontier in personalized care for heart transplant recipients, with the potential to tailor both screening and preventative therapeutic strategies to individual CAV risk profiles.

## Sources of Funding

Research reported in this publication was supported by the National Heart, Lung and Blood Institute of the National Institutes of Health under award numbers K08HL159344 – 01 and R01HL151277-01A1, by the National Cancer Institute under award number U01 CA239055-01, by the National Center for Advancing Translational Sciences of the National Institutes of Health under awards number KL2TR001879, and by the Gund Family Fund at the University of Pennsylvania.

The content is solely the responsibility of the authors and does not necessarily represent the official views of the National Institutes of Health or the United States Government.

## Disclosures

Dr. Eliot Peyster holds a patent related to the present work along with Drs. Feldman, Margulies, and Janowczyk (US patent # 10528848). Dr. Feldman is an equity holder and has technology licensed to both Elucid Bioimaging and Inspirata Inc. Dr. Janowczyk receives personal fees from Merck, and has patents issued (number 9111179) and pending (numbers 20190266726,



20190251687, 20180129911, and 20160307305) with the United States Patent and Trademark Office for computational image analysis and classification of pathology slides, and quality control of pathology slides. Dr. Feldman is a scientific advisory consultant for Inspirata Inc. and sits on its scientific advisory board. Dr. Feldman is also a consultant for Phillips Healthcare, XFIN, and Virbio. Dr. Margulies serves as a scientific consultant/advisory board member for Bristol-Myers-Squibb, NGM Biopharmaceuticals and DINAQOR Ltd, he has sponsored research agreements from Amgen, Inc. Ms. Swamidoss has nothing to disclose. Mr. Kethireddy has nothing to disclose.

## Supplemental Materials

Expanded Methods



Supplemental Figures 1-3

Supplemental Tables 1-10

## References

1. Lund LH, Edwards LB, Kucheryavaya AY, Benden C, Christie JD, Dipchand AI, Dobbels F, Goldfarb SB, Levvey BJ, Meiser B, et al. The registry of the International Society for Heart and Lung Transplantation: thirty-first official adult heart transplant report--2014; focus theme: retransplantation. *J Heart Lung Transplant*. 2014;33:996-1008.
2. Lund LH, Khush KK, Cherikh WS, Goldfarb S, Kucheryavaya AY, Levvey BJ, Meiser B, Rossano JW, Chambers DC, Yusen RD, et al. The Registry of the International Society for Heart and Lung Transplantation: Thirty-fourth Adult Heart Transplantation Report-2017; Focus Theme: Allograft ischemic time. *J Heart Lung Transplant*. 2017;36:1037-1046.
3. Bruneval P, Angelini A, Miller D, Potena L, Loupy A, Zeevi A, Reed EF, Dragun D, Reinsmoen N, Smith RN, et al. The XIIIth Banff Conference on Allograft Pathology: The Banff 2015 Heart Meeting Report: Improving Antibody-Mediated Rejection Diagnostics: Strengths, Unmet Needs, and Future Directions. *Am J Transplant*. 2017;17:42-53.
4. Chih S, Chong AY, Mielniczuk LM, Bhatt DL and Beanlands RSB. Allograft Vasculopathy: The Achilles' Heel of Heart Transplantation. *J Am Coll Card*. 2016;68:80-91.
5. Loupy A, Coutance G, Bonnet G, Van Keer J, Raynaud M, Aubert O, Bories M-C, Racapé M, Yoo D, Duong Van Huyen J-P, et al. Identification and Characterization of Trajectories of Cardiac Allograft Vasculopathy After Heart Transplantation. *Circulation*. 2020;141:1954-1967.
6. DePasquale EC. Predicting the Future of Cardiac Allograft Vasculopathy With Cardiac Positron Emission Tomography. *Circ Heart Fail*. 2018;11:e005136.
7. Eisen HJ, Tuzcu EM, Dorent R, Kobashigawa J, Mancini D, Valentine-von Kaeppeler HA, Starling RC, Sorensen K, Hummel M, Lind JM, et al. Everolimus for the prevention of allograft rejection and vasculopathy in cardiac-transplant recipients. *N Engl J Med*. 2003;349:847-58.
8. Hiemann Nicola E, Wellnhofer E, Knosalla C, Lehmkuhl Hans B, Stein J, Hetzer R and Meyer R. Prognostic Impact of Microvasculopathy on Survival After Heart Transplantation. *Circulation*. 2007;116:1274-1282.
9. Kaze AD, Santhanam P, Erqou S, Ahima RS, Bertoni A and Echouffo-Tcheugui JB. Microvascular Disease and Incident Heart Failure Among Individuals With Type 2 Diabetes Mellitus. *J. Am. Heart Assoc*. 2021;10:e018998.
10. Rush CJ, Berry C, Oldroyd KG, Rocchiccioli JP, Lindsay MM, Touyz RM, Murphy CL, Ford TJ, Sidik N, McEntegart MB, et al. Prevalence of Coronary Artery Disease and Coronary Microvascular Dysfunction in Patients With Heart Failure With Preserved Ejection Fraction. *JAMA Cardiology*. 2021;1;6(10):1130-1143
11. Climie RE, Sloten TTv, Bruno R-M, Taddei S, Empana J-P, Stehouwer CDA, Sharman JE, Boutouyrie P and Laurent S. Macrovasculature and Microvasculature at the Crossroads Between Type 2 Diabetes Mellitus and Hypertension. *Hypertension*. 2019;73:1138-1149.
12. Revelo MP, Miller DV, Stehlik J, Brunisholz K, Drakos S, Gilbert EM, Everitt M, Budge D, Alhareethi R, Snow G, et al. Longitudinal evaluation of microvessel density in survivors vs. nonsurvivors of cardiac pathologic antibody-mediated rejection. *Cardiovasc Pathol*. 2012;21:445-54.

13. Loupy A, Toquet C, Rouvier P, Beuscart T, Bories MC, Varnous S, Guillemain R, Pattier S, Suberbielle C, Leprince P, et al. Late Failing Heart Allografts: Pathology of Cardiac Allograft Vasculopathy and Association With Antibody-Mediated Rejection. *Am J Transplant.* 2016;16:111-20.
14. van den Hoogen P, Huijbers MMH, Sluijter JPG and de Weger RA. Cardiac allograft vasculopathy: a donor or recipient induced pathology? *J. Cardiovasc. Transl. Res.* 2015;8:106-116.
15. Gupta A, Broin PÓ, Bao Y, Pullman J, Kamal L, Ajaimy M, Lubetzky M, Colovai A, Schwartz D, de Boccardo G, et al. Clinical and molecular significance of microvascular inflammation in transplant kidney biopsies. *Kidney Int.* 2016;89:217-225.
16. Doreille A, Dieudé M and Cardinal H. The determinants, biomarkers, and consequences of microvascular injury in kidney transplant recipients. *Am. J. Physiol. Renal Physiol.* 2018;316:F9-F19.
17. Ishii Y, Sawada T, Kubota K, Fuchinoue S, Teraoka S and Shimizu A. Injury and progressive loss of peritubular capillaries in the development of chronic allograft nephropathy. *Kidney Int.* 2005;67:321-332.
18. Tsuji T, Yanai M, Itami H, Ishii Y, Akimoto M, Fukuzawa N, Harada H and Fukasawa Y. Microvascular inflammation in early protocol biopsies of renal allografts in cases of chronic active antibody-mediated rejection. *Nephrology (Carlton)*. 2015;20 Suppl 2:26-30.
19. Mehra MR, Crespo-Leiro MG, Dipchand A, Ensminger SM, Hiemann NE, Kobashigawa JA, Madsen J, Parameshwar J, Starling RC and Uber PA. International Society for Heart and Lung Transplantation working formulation of a standardized nomenclature for cardiac allograft vasculopathy&#x2014;2010. *J Heart Lung Transplant.* 2010;29:717-727.
20. López-Sainz Á, Barge-Caballero E, Barge-Caballero G, Couto-Mallón D, Paniagua-Martin MJ, Seoane-Quiroga L, Iglesias-Gil C, Herrera-Noreña JM, Cuenca-Castillo JJ, Vázquez-Rodríguez JM, et al. Late graft failure in heart transplant recipients: incidence, risk factors and clinical outcomes. *Eur J Heart Fail.* 2018;20:385-394.
21. Seki A and Fishbein MC. Predicting the development of cardiac allograft vasculopathy. *Cardiovasc Pathol.* 2014;23:253-60.
22. Mehra Mandeep R, Ventura Hector O, Chambers R, Collins Tyrone J, Ramee Stephen R, Kates Marc A, Smart Frank W and Stapleton Dwight D. Predictive model to assess risk for cardiac allograft vasculopathy: An intravascular ultrasound study. *J Am Coll Car.* 1995;26:1537-1544.
23. Watanabe K, Miyamoto SD and Nakano SJ. Predicting Cardiac Allograft Vasculopathy Using Circulating Vascular Endothelial Growth Factor in Pediatric Heart Transplant Recipients. *J Heart Lung Transplant.* 2017;36:S78-S79.
24. Sato T, Seguchi O, Ishibashi-Ueda H, Yanase M, Okada N, Kuroda K, Hisamatsu E, Sunami H, Watanabe T, Nakajima S, et al. Risk Stratification for Cardiac Allograft Vasculopathy in Heart Transplant Recipients – Annual Intravascular Ultrasound Evaluation –. *Circ J.* 2016;80:395-403.

25. Moayedi Y and Teuteberg JJ. Predicting Where Patients Will Be, Rather Than Just Seeing Where They Are. *Circulation*. 2020;141:1968-1970.
26. Alfonso F, Rivero F and Segovia-Cubero J. Early diagnosis of cardiac allograft vasculopathy: biopsy, liquid biopsy, non-invasive imaging, coronary imaging, or coronary physiology? *Eur Heart J*. 2021;42(48):4930-4933
27. Duong Van Huyen JP, Fedrigo M, Fishbein GA, Leone O, Neil D, Marboe C, Peyster E, von der Thüsen J, Loupy A, Mengel M, et al. The XVth Banff Conference on Allograft Pathology The Banff Workshop Heart Report: Improving the Diagnostic Yield from Endomyocardial Biopsies and Quilty Effect Revisited. *Am J Transplant*. 2020;(12):3308-3318.
28. Nirschl JJ, Janowczyk A, Peyster EG, Frank R, Margulies KB, Feldman MD and Madabhushi A. A deep-learning classifier identifies patients with clinical heart failure using whole-slide images of H&E tissue. *PLOS ONE*. 2018;13:e0192726.
29. Peyster EG, Arabyarmohammadi S, Janowczyk A, Azarianpour-Esfahani S, Sekulic M, Cassol C, Blower L, Parwani A, Lal P, Feldman MD, et al. An automated computational image analysis pipeline for histological grading of cardiac allograft rejection. *Eur Heart J*. 2021;42:2356-2369.
30. Peyster EG, Wang C, Ishola F, Remeniuk B, Hoyt C, Feldman MD and Margulies KB. In Situ Immune Profiling of Heart Transplant Biopsies Improves Diagnostic Accuracy and Rejection Risk Stratification. *J Am Coll Cardiol Basic Trans Science*. 2020;5:328-340.
31. Janowczyk A, Chandran S, Singh R, Sasaroli D, Coukos G, Feldman MD and Madabhushi A. High-Throughput Biomarker Segmentation on Ovarian Cancer Tissue Microarrays via Hierarchical Normalized Cuts. *IEEE Trans Biomed*. 2012;59:1240-1252.
32. Leo P, Shankar E, Elliott R, Janowczyk A, Madabhushi A and Gupta S. Combination of nuclear NF-kB/p65 localization and gland morphological features from surgical specimens is predictive of early biochemical recurrence in prostate cancer patients. *SPIE Medical Imaging*. 2018;10581:9.
33. Lu C, Lewis JS, Jr., Dupont WD, Plummer WD, Jr., Janowczyk A and Madabhushi A. An oral cavity squamous cell carcinoma quantitative histomorphometric-based image classifier of nuclear morphology can risk stratify patients for disease-specific survival. *Mod Pathol*. 2017;30:1655-1665.
34. Bulten W, Pinckaers H, van Boven H, Vink R, de Bel T, van Ginneken B, van der Laak J, Hulsbergen-van de Kaa C and Litjens G. Automated deep-learning system for Gleason grading of prostate cancer using biopsies: a diagnostic study. *Lancet Oncol*. 2020;21:233-241.
35. Ström P, Kartasalo K, Olsson H, Solorzano L, Delahunt B, Berney DM, Bostwick DG, Evans AJ, Grignon DJ, Humphrey PA, et al. Artificial intelligence for diagnosis and grading of prostate cancer in biopsies: a population-based, diagnostic study. *Lancet Oncol*. 2020;21:222-232.
36. Janowczyk A, Basavanhally A and Madabhushi A. Stain Normalization using Sparse AutoEncoders (StaNoSA): Application to digital pathology. *Comput Med Imaging Graph*. 2017;57:50-61.

37. Janowczyk A, Zuo R, Gilmore H, Feldman M and Madabhushi A. HistoQC: An Open-Source Quality Control Tool for Digital Pathology Slides. *JCO Clin Cancer Inform.* 2019;1-7.
38. Orosz CG and Pelletier RP. Chronic remodeling pathology in grafts. *Curr Opin Immunol.* 1997;9:676-80.
39. Booth AJ and Bishop DK. TGF-beta, IL-6, IL-17 and CTGF direct multiple pathologies of chronic cardiac allograft rejection. *Immunotherapy.* 2010;2:511-20.
40. Diaz JA, Booth AJ, Lu G, Wood SC, Pinsky DJ and Bishop DK. Critical role for IL-6 in hypertrophy and fibrosis in chronic cardiac allograft rejection. *Am J Transplant.* 2009;9:1773-83.
41. Schiechl G, Hermann FJ, Rodriguez Gomez M, Kutzi S, Schmidbauer K, Talke Y, Neumayer S, Goebel N, Renner K, Brühl H, et al. Basophils Trigger Fibroblast Activation in Cardiac Allograft Fibrosis Development. *Am J Transplant.* 2016;16:2574-88.
42. Colvin MM, Cook JL, Chang P, Francis G, Hsu DT, Kiernan MS, Kobashigawa JA, Lindenfeld J, Masri SC, Miller D, et al. Antibody-mediated rejection in cardiac transplantation: emerging knowledge in diagnosis and management: a scientific statement from the American Heart Association. *Circulation.* 2015;131:1608-39.
43. Lu WH, Palatnik K, Fishbein GA, Lai C, Levi DS, Perens G, Alejos J, Kobashigawa J and Fishbein MC. Diverse morphologic manifestations of cardiac allograft vasculopathy: a pathologic study of 64 allograft hearts. *J Heart Lung Transplant.* 2011;30:1044-50.
44. Loupy A, Duong Van Huyen JP, Hidalgo L, Reeve J, Racapé M, Aubert O, Venner JM, Falmuski K, Bories MC, Beuscart T, et al. Gene Expression Profiling for the Identification and Classification of Antibody-Mediated Heart Rejection. *Circulation.* 2017;135:917-935.
45. Ruifrok A and Johnston D. Ruifrok AC, Johnston DA. Quantification of histochemical staining by color deconvolution. *Anal Quant Cytol Histol* 23: 291-299. *Anal Quant Cytol Histol.* 2001;23:291-9.
46. Heinze G and Dunkler D. Five myths about variable selection. *Transpl Int.* 2017;30:6-10.
47. van Smeden M, Moons KGM, de Groot JAH, Collins GS, Altman DG, Eijkemans MJC and Reitsma JB. Sample size for binary logistic prediction models: Beyond events per variable criteria. *Stat Methods Med Res.* 2018;28:2455-2474.
48. Ariel Linden, 2015. "LOOCLASS: Stata module for generating classification statistics of Leave-One-Out cross-validation for binary outcomes," Statistical Software Components S458032, Boston College Department of Economics, revised 05 Nov 2020.
49. Liu X. Classification accuracy and cut point selection. *Stat Med.* 2012;31:2676-86.
50. Smits JM, De Pauw M, de Vries E, Rahmel A, Meiser B, Laufer G and Zuckermann A. Donor scoring system for heart transplantation and the impact on patient survival. *J Heart Lung Transplant.* 2012;31:387-97.
51. Nagji AS, Hranjec T, Swenson BR, Kern JA, Bergin JD, Jones DR, Kron IL, Lau CL and Ailawadi G. Donor age is associated with chronic allograft vasculopathy after adult heart transplantation: implications for donor allocation. *Ann Thorac Surg.* 2010;90:168-175.

52. Peyster EG, Madabhushi A and Margulies KB. Advanced Morphologic Analysis for Diagnosing Allograft Rejection: The Case of Cardiac Transplant Rejection. *Transplantation*. 2018;102:1230-1239.
53. Dooley AE, Tong L, Deshpande SR and Wang MD. Prediction of Heart Transplant Rejection Using Histopathological Whole-Slide Imaging. *IEEE EMBS Int Conf Biomed Health Inform*. 2018;10:1109.
54. Jeffrey J, Nirschl AJ, Eliot G, Peyster, Renee Frank, Kenneth B, Margulies, Michael D, Feldman, Anant Madabhushi. Deep Learning Tissue Segmentation in Cardiac Histopathology Images. In: H. G. S. Kevin Zhou, Dinggang Shen, ed. *Deep Learning for Medical Image Analysis*; 2017:179-195.
55. Colvin MM, Cook JL, Chang P, Francis G, Hsu DT, Kiernan MS, Kobashigawa JA, Lindenfeld J, Masri SC, Miller D, et al. Antibody-Mediated Rejection in Cardiac Transplantation: Emerging Knowledge in Diagnosis and Management. *Circulation*. 2015;131:1608-1639.



# Circulation

**Table 1:** Clinical, histologic, and donor characteristics of early cardiac allograft vasculopathy patients, as compared to patients without allograft vasculopathy:

	No -CAV (n=249)	PrE-CAV (n=53)	p Value (univariate)
<b><u>RECIPIENTS:</u></b>			
• Age at OHT (yrs)	52.6	48.9	<b>0.020</b>
• Sex (% Female)	23.6	21.2	0.604
• White Ethnicity (%)	83.6	78.8	0.452
• BMI at 1yr post OHT	28.0	29.8	<b>0.033</b>
<b><u>Medical History</u></b>			
• Hypertension (%)	80.3	82.7	0.699
• Hyperlipidemia (%)	82.2	86.5	0.472
• Diabetes Mellitus (%)	57.5	75.0	<b>0.042</b>
• Coronary Artery Disease	39.4	40.4	0.665
• CMV IgG Positive (%)	42.9	50.9	0.343
• CMV infection in 1 <sup>st</sup> year	6.0	15.1	<b>0.024</b>
<b><u>Histology History:</u></b>			
• Average ISHLT Grade of prior EMBs at 1 yr*	0.71	0.78	0.163
• % of Prior EMBs with Quilty at 1yr*	13.2	23.0	<0.001
• Treated Acute Rejection <sup>†</sup> in 1 <sup>st</sup> yr (%)	44.3	50.0	<b>0.002</b>
• History of Positive PRA/CPRA (% of patients)	20.8	13.2	0.200
• Positive Donor Specific Antibody in 1 <sup>st</sup> yr (%)	11.2	11.3	0.987
• LDL Cholesterol at 1yr post OHT (mg/dL)	85.4	103.4	<0.001
• Average LVEF at 1 year post OHT (%)	65.0	64.1	0.881
<b><u>DONORS:</u></b>			
• Age (yrs)	39.1	40.0	0.676
• Sex (% Female)	37.8	35.6	0.754
• White Ethnicity (%)	75.6	73.1	0.624
• Smoking History (%)	22.8	33.9	0.097
• BMI	28.0	27.7	0.875
• Hypertension (%)	22.8	22.6	0.919
• Diabetes (%)	8.2	7.6	0.610
• Coronary Angiography Score <sup>‡</sup>	2.2	2.8	0.093

• Median Heart Donor Score <sup>50</sup>	16.8	17.1	0.801
• Organ Ischemic Time (avg, minutes)	190.5	185.6	0.849
• Proteinuria at Harvest (%)	42.1	56	0.072
• LVEF at Harvest (%)	60.8	61.0	0.922
• Average number of HLA Mismatches	4.5	4.7	0.849
• CMV Mismatch [Donor(-)/Recipient(+)]	28.8	28.9	0.808
• Sex Mismatch ( $\text{♀}$ donor to $\text{♂}$ recipient)	21.6	23.1	0.879
• Race Mismatch	35.2	45.3	0.079
• Serum BUN:Creatinine Ratio (average)	14.8	13.8	0.340

\*These are per-patient averages

† Treated acute rejection refers to any treated rejection event, regardless of grade or sub-type.

‡ Coronary Angiography Score is derived from the validated EuroTransplant Heart Donor Score<sup>50</sup>, and assumes the lowest score for donors 34 years of age and younger if no angiography is performed at harvest.

PrE-CAV = pre-early cardiac allograft vasculopathy (CAV) patients, defined as patients experiencing overt CAV by 5-years post-transplant but without overt diagnosis at 1-year post-transplant. No-CAV = patients without overt CAV at 6-years post-transplant. OHT = orthotopic heart transplant, ISHLT = international society for heart and lung transplantation, LVEF= Left ventricular ejection fraction, BMI = body mass index, LDL= low density lipoprotein, CMV= cytomegalovirus.



**Table 2:** Histologic characteristics of the endomyocardial biopsy cases used for automated histologic analysis

	No-CAV (n=82)	PrE-CAV	Disease Controls
<b>Days post-transplant biopsy obtained (average)</b>	365	358	2350
<b>ISHLT Grade 0R (n)</b>	41% (34)	24% (12)	35.3% (18)
<b>ISHLT Grade 1R (n)</b>	57.8% (48)	76% (38)	64.7% (33)
<b>ISHLT Grade 2R/3R (n)</b>	0%	0%	0%
<b>Quilty Lesion (n)</b>	6% (5)	30% (15)	15.7% (8)
<b>Prior Biopsy Changes (n)</b>	6% (5)	6% (3)	3.9% (2)
<b>C4d+ on Immunofluorescene staining<sup>§</sup> (n)</b>	0%	0%	19.6% (10)
<b>Immunopathologic Antibody Mediated Rejection / pAMR1-i+ (n)</b>	0%	0%	3.9% (2)
<b>Digitized on Hamatsu slide scanner (vs. Aperio)</b>	60% (49)	60% (30)	54.9% (28)

ISHLT = International Society for Heart and Lung Transplantation.

§C4d+ on IF staining describes any positive staining, even if insufficient for a diagnosis of antibody mediated rejection/pAMR-i+.

pAMR1-i+ = ISHLT grade 1 with immunofluorescence sufficiently positive to be consistent with antibody mediated rejection (AMR).

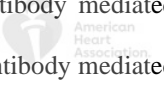


## Figure Legends

### Figure 1: Flow Diagram for Cardiac Allograft Vasculopathy (CAV) Experiments.

N=746 transplant recipients from the University of Pennsylvania between 2007-2020 underwent detailed health record review to collect baseline data at time of transplant, donor data, 1-year-post-transplant clinical data, and long-term CAV outcomes data. Patients were labeled as ‘No-CAV’ if they did not have any evidence of CAV by six-years-post-transplant, and were labeled as ‘Pre-Early-CAV’ (PrE-CAV) if they developed moderate or severe CAV by five-years post-transplant (but not before 1-year post-transplant). N=444 did not meet either definition, due to lack of CAV diagnosis (thus not meeting PrE-CAV definition), or due to <6 years of follow-up (thus unable to meet No-CAV definition). N=302 patients met a study group definition, and were included in study analyses. Based on clinical data available at 1-year post-transplant, a clinical risk factor model for predicting future CAV was developed to distinguish between No-CAV and PrE-CAV patients (the ClinCAV-Pr model). Additionally, n=183 archival biopsies from study patients were collected, stained, and digitized to undergo digital pathology image analysis for ‘morphologic biomarker’ extraction. ‘PrE-CAV biopsies’ and ‘No-CAV biopsies’ were comprised of low-grade, one-year post-transplant surveillance biopsy tissues, while ‘Disease-Control’ (DC) biopsies were biopsies obtained from patients at the time of definitive moderate/severe CAV diagnosis. Morphologic biomarker models were developed to distinguish between overt CAV biopsies and No-CAV biopsies (the HistoCAV-Dx model) and to predict future CAV development based on 1-year post-transplant No-CAV and PrE-CAV biopsies (the HistoCAV-Pr model). Finally, to test the added predictive value of novel morphologic biomarkers, clinical risk factors and morphologic biomarkers were combined in an integrated ‘iCAV-Pr’ model.



**Figure 2: Example Digital Histology Images for 1-year Post-transplant Biopsies from Pre-Early CAV (PrE-CAV) Patients Prior to Disease Onset and 1-year Post-transplant from Non-early CAV (No-CAV) Patients, as well as Disease Control (DC) Biopsies Obtained from CAV Patients at the Time of Definitive Disease Diagnosis.**

Note the progressive interstitial/stromal changes in Movat's images for both DC and PrE-CAV patients, with prominent collagen (yellow) expansion in the DC EMBs. Also note the perivascular cellular density in PrE-CAV and DC biopsies, as well as notable increases in thickness of the DAB (brown) stain in the CD31 DC image suggesting endothelial cell hypertrophy or proliferation. These and other, subtler features were extracted from these images during image analysis, and used to develop the experimental Histologic Diagnostic and Predictive models for CAV (histoCAV-Dx and HistoCAV-Pr, respectively).



**Figure 3: Image Analysis Workflow for Cardiac Allograft Vasculopathy Diagnosis and Prediction from Endomyocardial Biopsy Samples.**

Top row shows the workflow for CD31 stained slides, starting with a raw digital image and proceeding left to right with detection of CD31 stained vascular objects (dark brown in raw image, solid green after object detection and segmentation), color-unmixing and optical density algorithms to resolve nuclei (blue) underlying CD31 vascular objects, nuclear object detection and segmentation both in and around these vascular objects, and finally, differentiation of perivascular (blue) vs. intra-vascular (red) nuclei for deeper characterization of vascular morphology changes. Bottom row shows the workflow for the corresponding Movats stained slides. The first segmentation steps identify all stromal fibers (both mucopolysaccharides/glycosaminoglycans [GAGs] in darker green and collagen in lighter green) and all myocytes (red). This is followed by generation of a 'myocardial mask' which encompasses the tissue compartment containing significant myocyte density, and sub-analysis of the stromal fibers contained within this myocardial mask to quantify and contrast interstitial stromal changes with more global stromal findings.

**Figure 4: Visual Examples with Explanatory Descriptions of Morphologic Biomarker Categories that Comprise the Histologic Cardiac Allograft Vasculopathy Diagnostic (HistoCAV-Dx) and Predictive (HistoCAV-Pr) Models.**

1st Row: increased interstitial collagen content (green arrows pointing to yellow staining between red myocytes) in a disease control (DC) tissue sample obtained at the time of definitive cardiac allograft vasculopathy (CAV) diagnosis (right image right) vs. a No-CAV tissue sample (left image panel), as seen in a Movats pentachrome stained slide. 2nd Row: Increased non-collagen interstitial stromal content (green arrows pointing to blue-grey staining between red myocytes) in a pre-early-CAV tissue sample (PrE-CAV) vs. a No-CAV sample (Movats pentachrome). Note that PrE-CAV and No-CAV samples are obtained at 1-year post-transplant, and that PrE-CAV samples are obtained before overt CAV onset. 3rd Row: Increased thickness of CD31 staining in vascular structures (green arrows pointing to brown areas), likely representing increased endothelial cell thickening/abundance in a DC sample vs. a No-CAV sample (CD31 stained slide). 4th Row: Increased cellularity (green arrows pointing to blue nuclei) within CD31 vascular structures (brown) in a DC sample vs. No-CAV (CD31 stained slide). 5th Row: Increased cellularity (green arrows pointing to blue nuclei) in the perivascular area immediately surrounding CD31 vascular structures (brown), as seen in a PrE-CAV sample vs. a No-CAV sample (CD31 stained slide). 6th Row: Area of decreased overall ‘vascular density’, with sparser brown-staining CD31 vascular structures in a DC sample vs. a No-CAV sample (CD31 stained slide).

**Figure 5: HistoCAV-Dx, a Model for Diagnosing Cardiac Allograft Rejection (CAV) Using Automated Image Analysis of Endomyocardial Biopsy (EMB) Tissues, was Trained on n=88 EMBs.**

Excellent diagnostic performance was achieved in an independent test set of n=45 EMBs, with area under the receiver operating characteristic curve and sensitivity both in excess of 90% for differentiating tissue from patients with CAV vs. those without CAV.

**Figure 6: Results for Three Experimental Models Designed to Predict Early/Aggressive Cardiac Allograft Vasculopathy (CAV) before Overt Disease Onset Using only Data Available at One-year Post-transplant.**

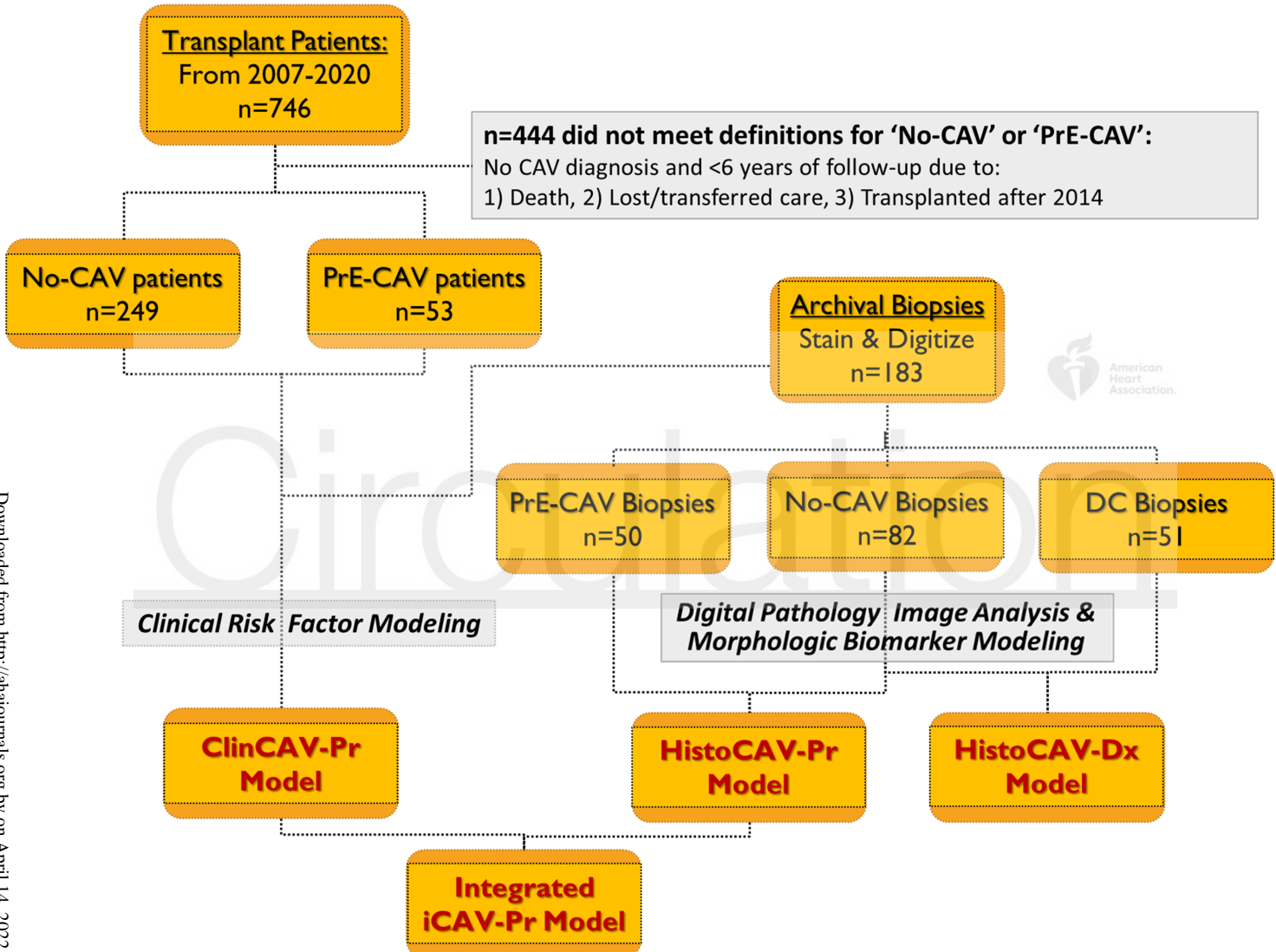
Left Column: Performance of the Clinical risk factor Prediction Model (ClinCAV-Pr) for predicting CAV in an independent test set (n=95 patients) after model training using clinical data from n=207 patients. Overall, this seven-variable model relying on clinical risk factors achieves modest predictive performance, though with a poor true positive rate and a true negative rate that largely benefits from an imbalanced cohort with a relatively low frequency of CAV. Middle Column: Performance of a Histologic Prediction Model (HistoCAV-Pr) for predicting CAV, based on automated histologic analysis of one-year post-transplant endomyocardial biopsies (EMB). After model training on n=88 EMBs, the model performance was assessed on an independent test set of n=44 EMBs corresponding to cases present in the ClinCAV-Pr test-set described above. Overall, good performance was achieved by the HistoCAV-Pr, with clear improvements in area under the ROC curve, accuracy, sensitivity, and positive predictive value compared to ClinCAV-Pr. Right Column: Performance of an Integrated ‘histo-clincal’ CAV prediction model (iCAV-Pr) for predicting CAV, which combines the prediction outputs of



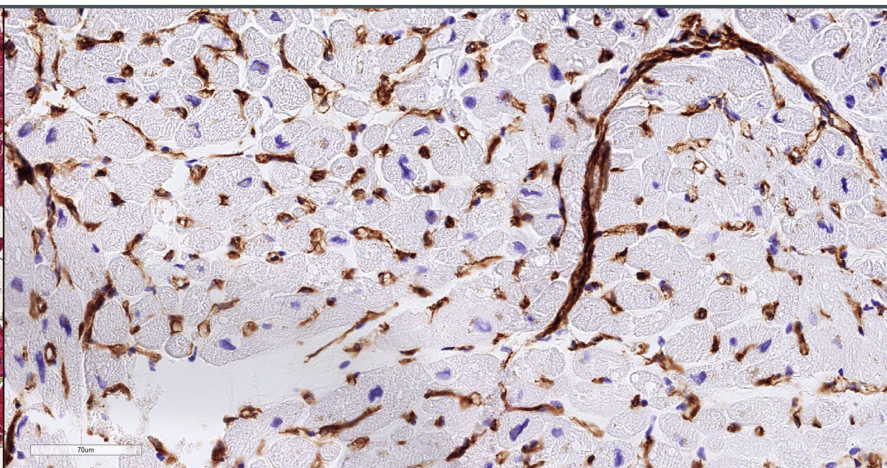
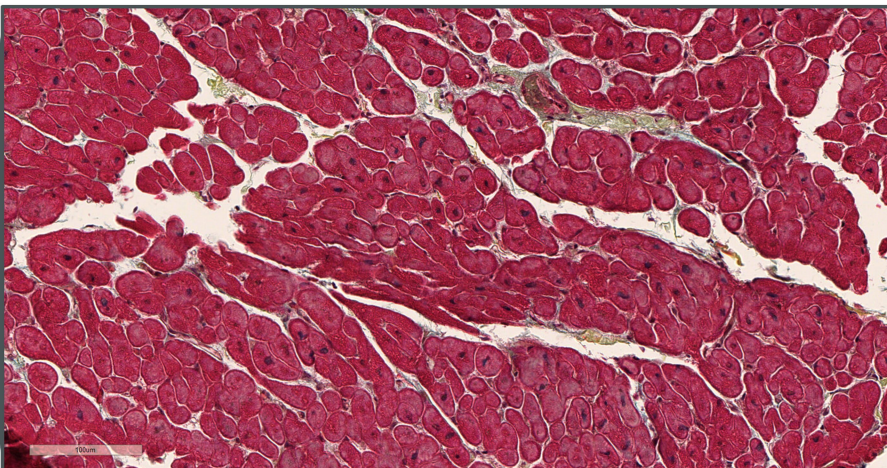
ClinCAV-Pr and HistoCAV-Pr. There is clear synergy when combining broad clinical risk factors and computationally extracted morphologic biomarkers, with excellent predictive performance that exceeds either model alone.



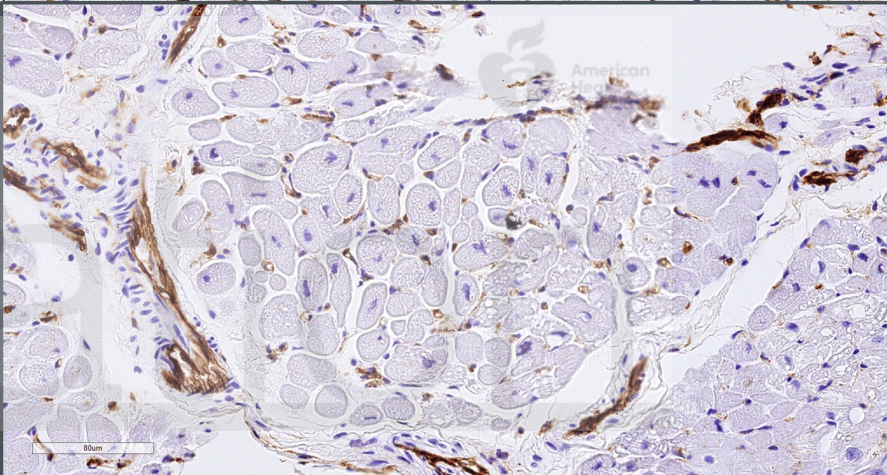
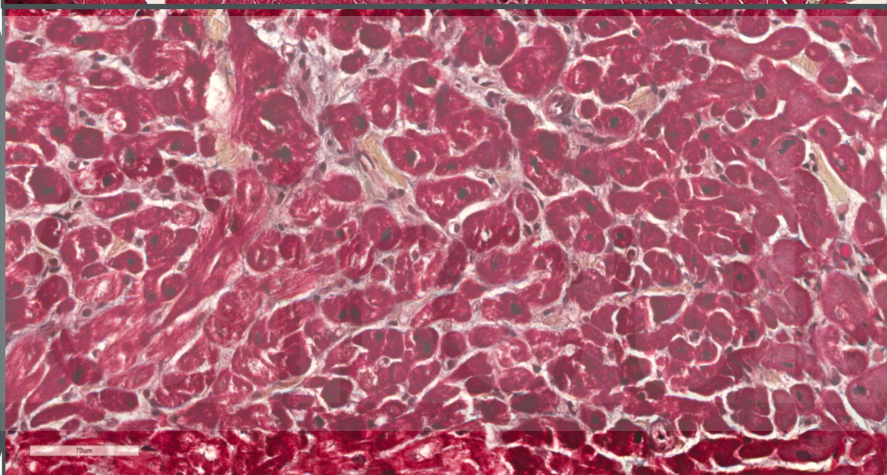
# Circulation



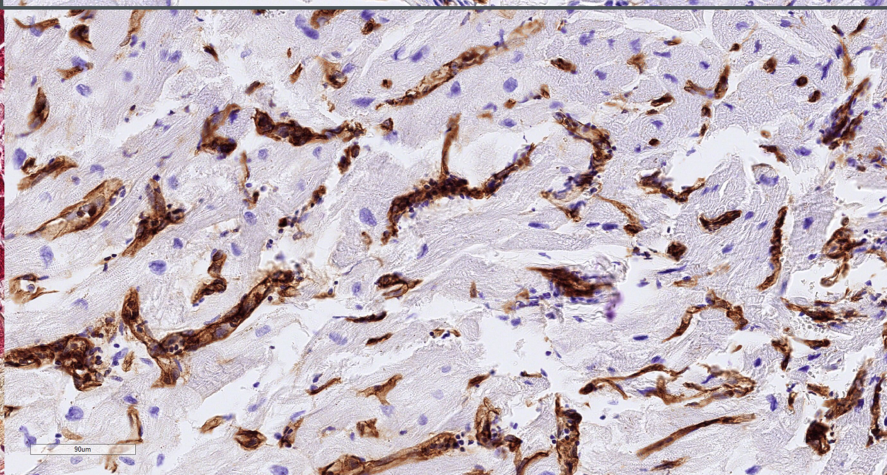
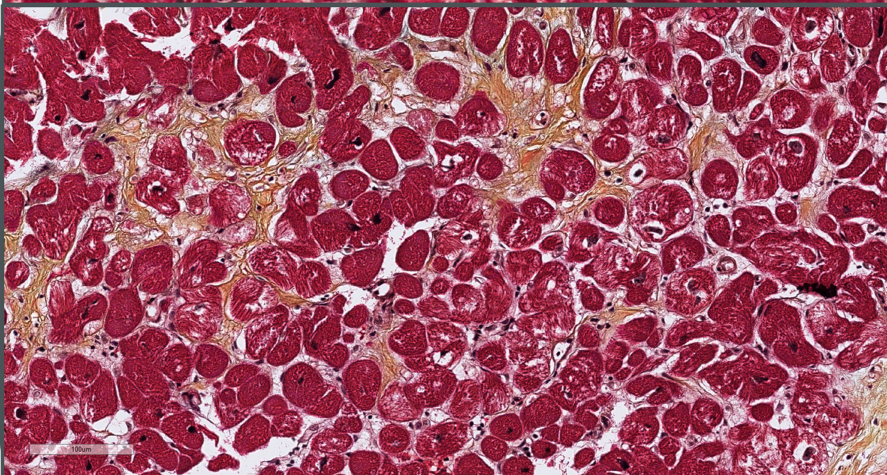
**No  
CAV  
Biopsy**

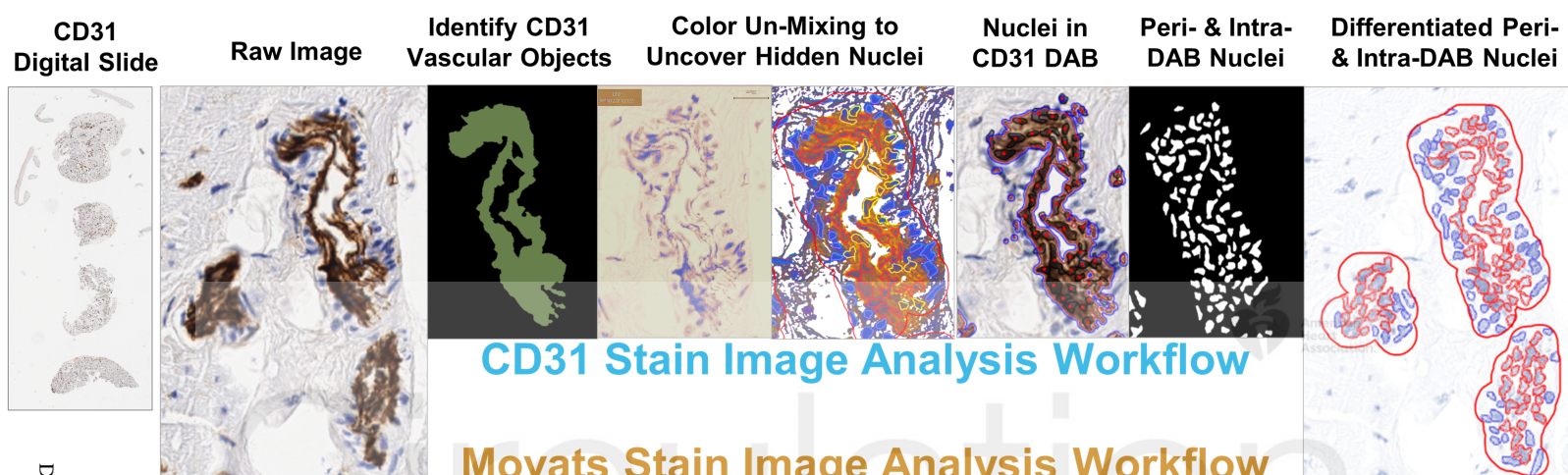


**Pre-  
Early  
CAV  
Biopsy**

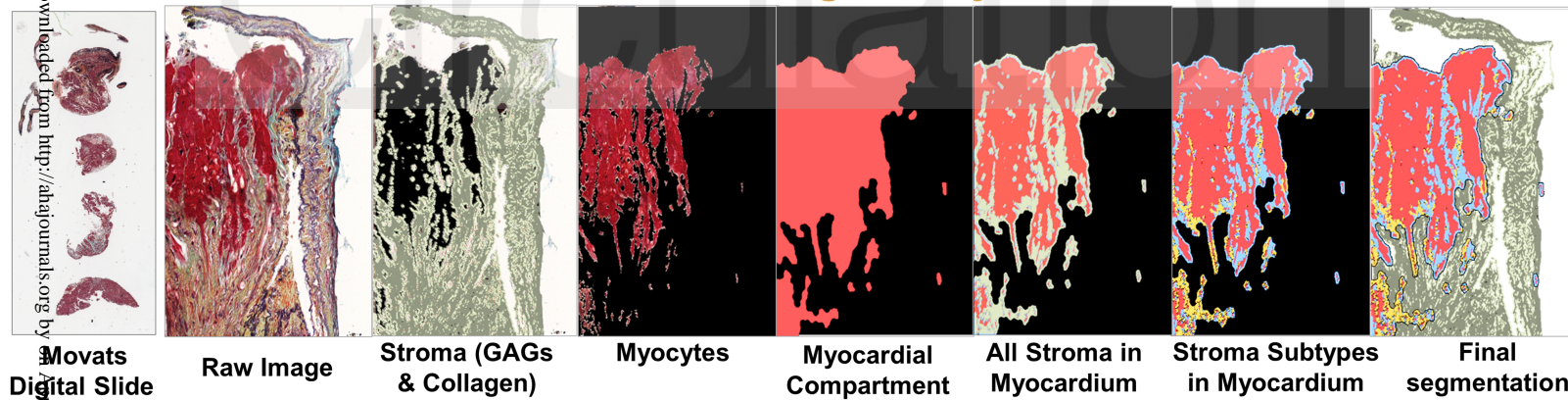


**Disease  
Control  
Biopsy**





### Movats Stain Image Analysis Workflow

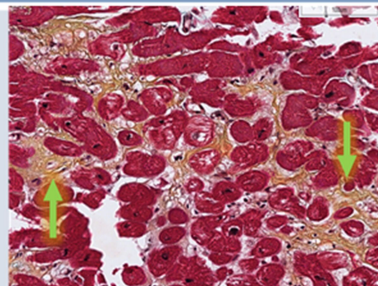
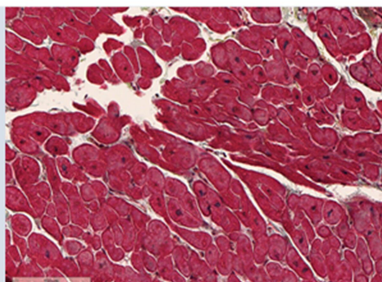


## Morphologic Biomarker Description

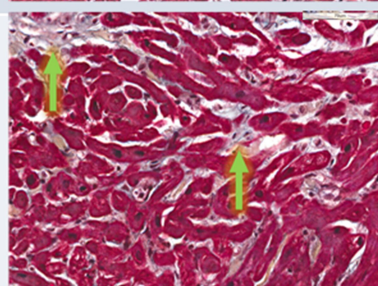
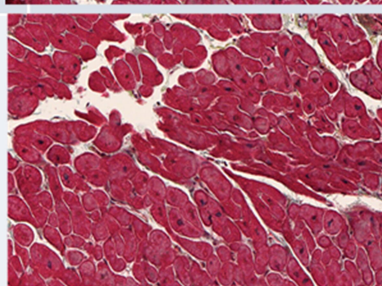
## No-CAV Slide

## PrE-CAV or DC Slide

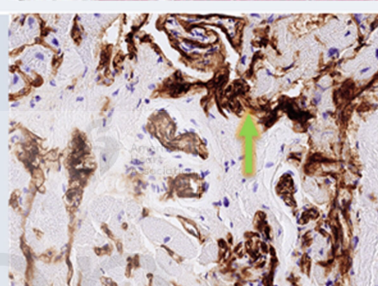
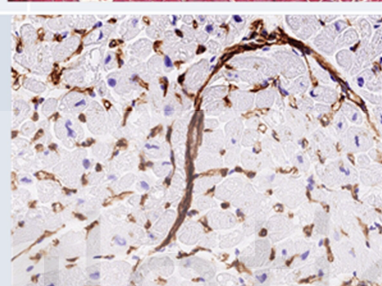
↑ Interstitial Stroma Proliferation  
(Collagen)



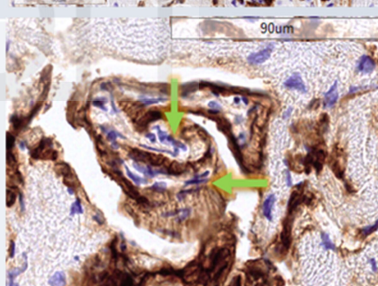
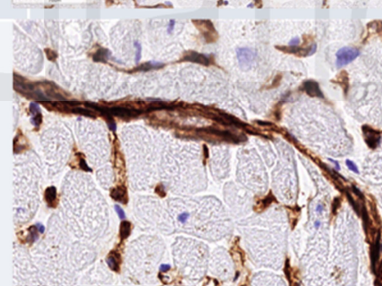
↑ Interstitial Stromal Proliferation  
(Non-Collagen)



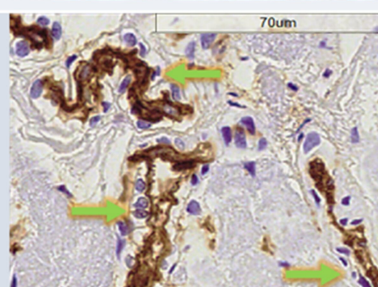
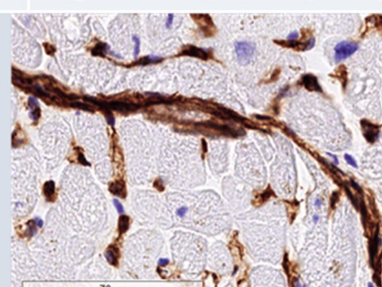
↑ Endothelial Cell  
Thickening/Abundance



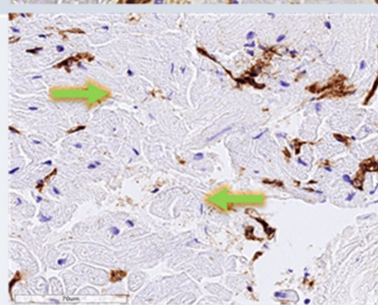
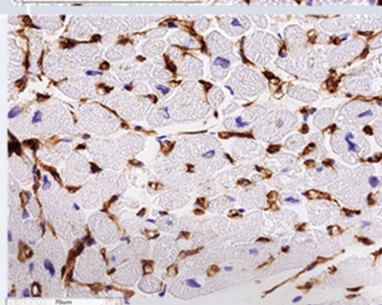
↑ Cellularity within Vascular  
Objects

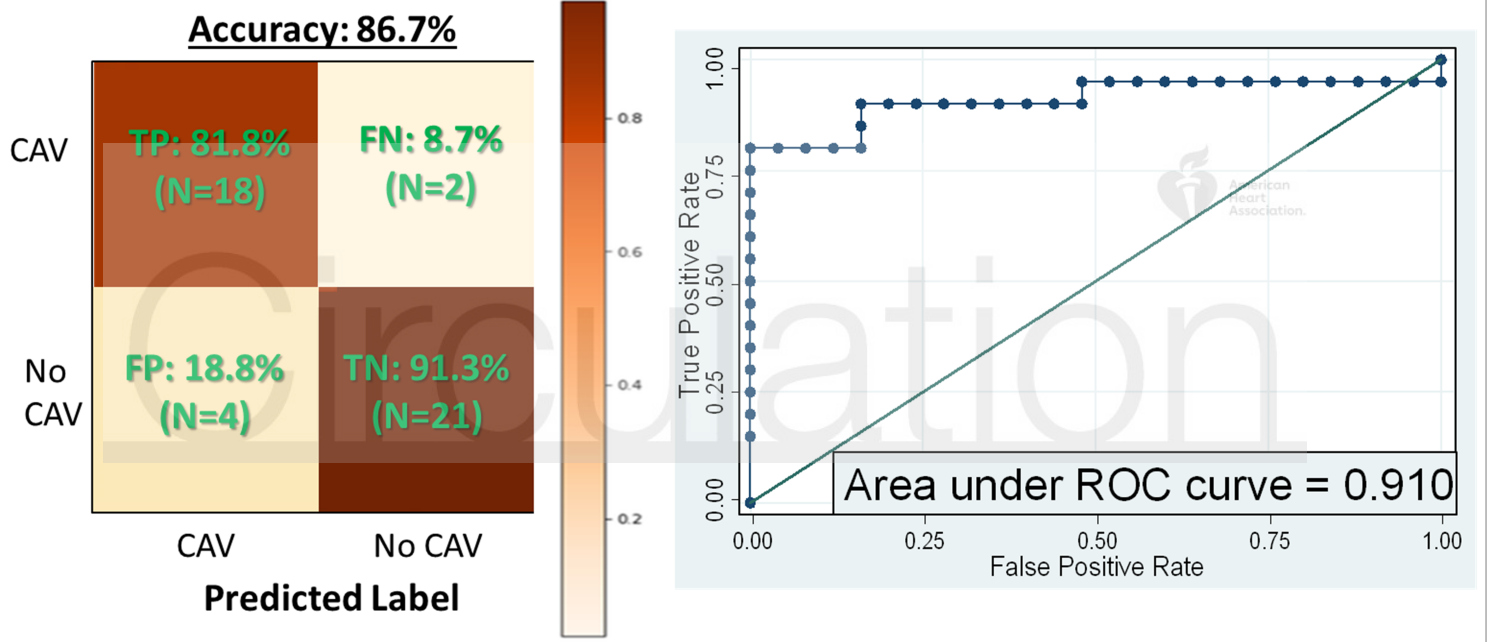


↑ Cellularity of Perivascular Space



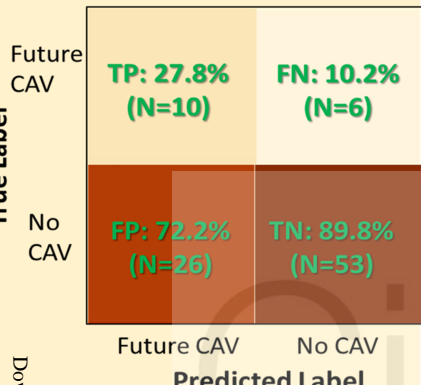
↓ Vascular Density





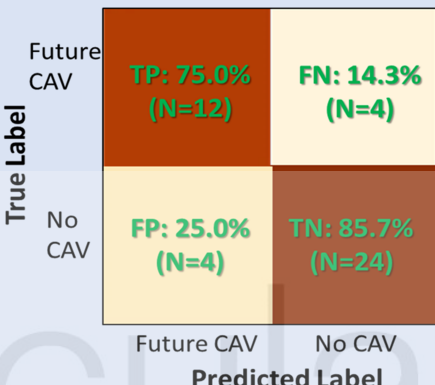
### Clinical CAV Prediction Model

Accuracy: 66.3%



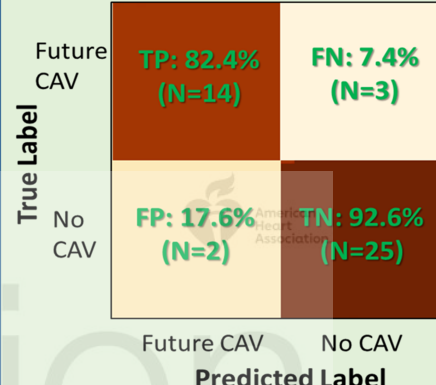
### Histologic CAV Prediction Model

Accuracy: 81.6%

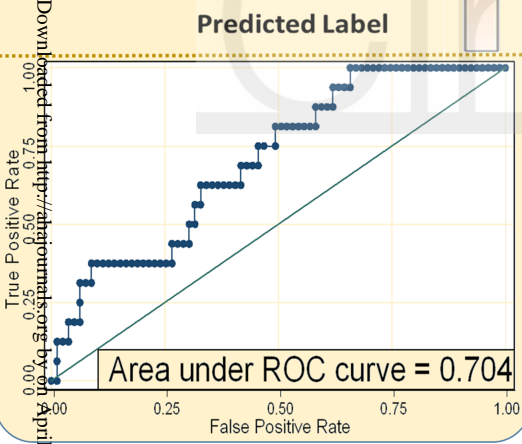


### Integrated 'Histo-Clinical' Model

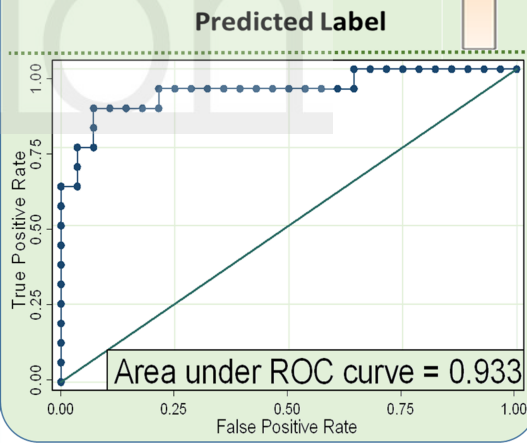
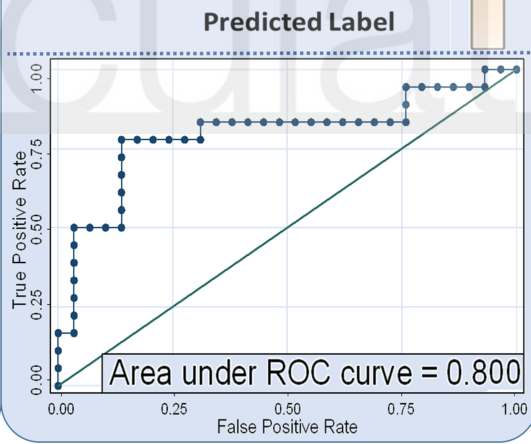
Accuracy: 88.6%



True Label



True Label



American Heart Association